Available online at www.sciencedirect.com
ScienceDirect
Journal of Solid State Chemistry 181 (2008) 964–970
JOURNAL OF SOLID STATE CHEMISTRY
www.elsevier.com/locate/jssc

Synthesis, crystal structure, and photocatalytic activity of a new two-layer Ruddlesden–Popper phase, $Li_2CaTa_2O_7$

Zhenhua Liang[a,b], Kaibin Tang[a,b,*], Qian Shao[a,b], Guocan Li[a,b], Suyuan Zeng[a,b], Huagui Zheng[b]

[a]*Nanomaterial and Nanochemistry, Hefei National Laboratory for Physical Sciences at Microscale, University of Science and Technology of China, Hefei, Anhui 230026, PR China*

[b]*Department of Chemistry, University of Science and Technology of China, Hefei, Anhui 230026, PR China*

Received 26 November 2007; received in revised form 14 January 2008; accepted 21 January 2008
Available online 13 February 2008

Abstract

A new two-layer Ruddlesden–Popper phase $Li_2CaTa_2O_7$ has been synthesized for the first time. The detailed structure determination of $Li_2CaTa_2O_7$ performed by powder X-ray diffraction (XRD) and electron microscopy (ED) shows that it crystallizes in the space group *Fmmm* [$a\sim5.5153(1)$, $b\sim5.4646(1)$, $c\sim18.2375(3)$Å]. UV–visible diffuse reflection spectrum of the prepared $Li_2CaTa_2O_7$ indicates that it had absorption in the UV region. The photocatalytic activity of the $Li_2CaTa_2O_7$ powders was evaluated by degradation of RhB molecules in water under ultra visible light irradiation. The results showed that $Li_2CaTa_2O_7$ has high photocatalytic activity at room temperature. Therefore, the preparation and properties studies of $Li_2CaTa_2O_7$ with a two-layer Ruddlesden–Popper structure suggest potential future applications in photocatalysis.

Keywords: Perovskite; Ruddlesden–Popper phase; Powder X-ray diffraction; Photocatalysis

1. Introduction

Recently there has been a growing interest in the study of layered perovskites, which possess a wide variety of interesting properties including superconductivity [1], colossal magnetoresistance [2], ferroelectricity [3], and catalytic activity [4]. Layered perovskites are intergrowths of perovskite and other structures, and they consist of two-dimensional perovskite slabs interleaved with cations or cationic structural units. Dion–Jacobson, Ruddlesden–Popper phases, and Aurivillius phases form the major families of closely related layered perovskites. The Dion–Jacobson series of layered perovskites, $A'[A_{n-1}B_nO_{3n+1}]$ [5], such as the $n=2$ phase $RbLaNb_2O_7$, has one interlayer cation per formula unit. Ruddlesden–Popper phases, $A'_2[A_{n-1}B_nO_{3n+1}]$ [6], typified by $Na_2La_2Ti_3O_{10}$, have two interlayer cations per formula unit and possess twice the interlayer charge density of the Dion–Jacobson phases. Aurivillius phases, $Bi_2O_2[A_{n-1}B_nO_{3n+1}]$ [7], including $Bi_2W_2O_9$ to emphasize the location of the bismuth oxide in the interlayer, are intergrowths of perovskite and bismuth oxide and have a covalent network of $(Bi_2O_2)^{2+}$ between the two-dimensional perovskite slabs. There is always a look-out for new members of these families because of the interesting properties they exhibit such as ion-exchange [8], intercalation [9], and catalysis [10] can be controlled depending on the choice of *A*- and *B*-site cations.

Among various applications of layered perovskites, the photocatalytic activity is one of the most challenging, as it can potentially provide clean and renewable sources for hydrogen fuel in the future. Since TiO_2 electrode was first studied for water decomposition under UV-light irradiation, a variety of photocatalysts, mainly Ti [11], Nb [12], and Ta [13–16] based oxides, have been reported to be

*Corresponding author at: Nanomaterial and Nanochemistry, Hefei National Laboratory for Physical Sciences at Microscale, University of Science and Technology of China, Hefei, Anhui 230026, PR China.
E-mail address: kbtang@ustc.edu.cn (K. Tang).

0022-4596/$ - see front matter © 2008 Published by Elsevier Inc.
doi:10.1016/j.jssc.2008.01.042

effective for photocatalytic decomposition of water. Sayama et al. [12] first demonstrated the use of ion-exchangeable layered oxides, $K_4Nb_6O_{17}$ and $K_2La_2Ti_3O_{10}$, as effective photocatalysts for water splitting. It was explained that these layered materials use their interlayer space as reaction sites, where the electron–hole recombination process could be retarded by physical separation of electron and hole pairs generated by photoabsorption. On the other hand, Ta-based catalysts have recently been developed as a new class of photocatalyst. Kudo et al. first studied the photocatalytic properties of many Ta-based catalysts, such as $Sr_2Ta_2O_7$ [14] and $NaTaO_3$ [15].

$A_2SrTa_2O_7$ (A = H, Li, K, and Rb)-type tantalates are new members of the Ruddlesden–Popper-type layered perovskite [17,18]. These materials are composed of layers of Sr–Ta perovskite sheets and potassium ions located in the interlayer. $A_2SrTa_2O_7$ materials act as new Ta-based photocatalysts with two-dimensional structures in water. Nevertheless, no member of this series that contains Ca^{2+} at A sites has been synthesized by the solid-state reaction.

In this paper, we report the first successful example of layered perovskite-type tantalates $Li_2CaTa_2O_7$, as very active photocatalysts. Detailed powder X-ray diffraction and electron microscopy study of $Li_2CaTa_2O_7$ shows that this phase crystallizes in the space group *Fmmm*, similar to the structure of $Li_2SrNb_2O_7$ [18]. Photocatalytic activity is characterized by diffuse reflectance UV spectroscopy, photoluminescence spectroscopy, and degradation of RhB molecules in water under ultra visible light irradiation as a test reaction.

2. Experimental section

2.1. Preparation of $Li_2CaTa_2O_7$ samples

$Li_2CaTa_2O_7$ powders were prepared by a conventional solid-state reaction. All reagents were analytically pure and used without further purification. Stoichiometric amounts of $CaCO_3$ and Ta_2O_5 with a 10% molar excess of Li_2CO_3 were mixed together and heated in air at 1200 °C for 2 h. The calcination procedure was repeated two times after grinding to ensure a complete reaction.

2.2. Samples characterizations

Samples of $Li_2CaTa_2O_7$ were characterised by powder X-ray diffraction recorded on a Philips X'Pert Pro Super diffractometer with Cu$K\alpha$ radiation ($\lambda = 1.54178$ Å) at room temperature (40 kV, 30 mA) in the angular range $5 < 2\theta < 110°$. The X-ray diffraction (XRD) data for indexing and cell-parameter calculation were collected in a continuous scan mode with a step size of 0.017°. The XRD patterns were analyzed by the Rietveld method using the FULLPROF program [19].

Morphologies and structures of the prepared samples were further examined with high-resolution transmission electron microscopy (HRTEM) images and electron diffraction (ED) patterns, which were carried out on a JEOL-2010 transmission electron microscope at an acceleration voltage of 200 kV. Samples used for HRTEM characterization were dispersed in absolute ethanol and were ultrasonicated before observation, and then a drop of the diluted colloidal suspension of the sample was placed onto a Cu grid. After being air-dried, the specimen was subjected to HRTEM observations. UV–vis diffuse reflectance spectrums (DRS) of the samples were measured using a Hitachi U-3010 UV–vis spectrophotometer. Photoluminescence was measured at 25 °C by a fluorometer (HITACHI F-4500).

2.3. Photocatalytic test

Photocatalytic activities of the $Li_2CaTa_2O_7$ powder were evaluated by the degradation of rhodamine-B under ultra visible light irradiation of a 450 W Hg lamp. In each experiment, 100.0 mg of as-prepared $Li_2CaTa_2O_7$ powder as a photocatalyst was added into 200 mL of rhodamine-B solution (2×10^{-5} mol/L). After being dispersed in an ultrasonic bath for 5 min, the solution was stirred for 30 min in the dark to reach adsorption equilibrium between the catalyst and the solution and then was exposed to photo irradiation. Concentrations of rhodamine-B were carried out using UV–vis spectra (Shimadzu UV2550) every 5 min.

3. Results and discussion

3.1. Synthesis of $Li_2CaTa_2O_7$

The synthesis of $Li_2CaTa_2O_7$ layered perovskite can be challenging because the small ionic radius of Ca^{2+} does not cooperate well in the perovskite structure. The ionic radius of Ca^{2+} is 1.34 Å (coordination number, CN = 12) and Ta^{2+} is 0.74 Å (coordination number, CN = 6), according to the ionic radii suggested by Shannon [20]. The tolerance factor of the perovskite structure is calculated using the following formula:

$$t = (R_A + R_B)/2(R_B + R_O), \quad (1)$$

where R_A, R_B, and R_O are the ionic radii of atoms in the A, B, and O sites, respectively, according to the formula of Ruddlesden–Popper phases, $A'_2[A_{n-1}B_nO_{3n+1}]$. The value of R_O is 1.40 Å (coordination number CN = 6) [20], and the calculated tolerance factor is 0.69, which is below the stable range (0.77–1.10) for the perovskite structure, indicating that the structure of $Li_2CaTa_2O_7$ is metastable and easy to collapse. Likewise, there are often competing phases that are more stable than the desired layered perovskite. To successfully synthesize $Li_2CaTa_2O_7$ layered perovskites, we optimized a synthetic approach of iterative brief heating and regrinding that stabilized the target phase relative to the competing kinetically and thermodynamically stable phases.

To investigate the two-layer Ruddlesden–Popper structure form, several experiments through intercepting the intermediate products were performed in the different stages of 4, 6 and 8 h. The intermediate products were inspected by XRD, as shown in Fig. 1. In the initial stage (4 h), the samples formed the primary two-layer Ruddlesden–Popper structure. However, the reaction was not completed and some weak peaks were exhibited in the XRD pattern, indicating there were still some reactants. As the reaction proceeded (6 h), the peaks in the XRD pattern became sharp and strong without any other peaks belonging to impurity, suggesting that the orthorhombic phase $Li_2CaTa_2O_7$ had crystallized well at this stage. All peaks can be indexed on an orthorhombic cell [$a\sim5.5157(3)$, $b\sim5.4652(3)$, $c\sim18.2338(9)$ Å] similar to $Li_2SrNb_2O_7$ [19]. When the reaction time increased to 8 h, the two-layer Ruddlesden–Popper structure started to collapse. All peaks of the impurity in the XRD pattern can be indexed on a tetragonal cell with $a = 3.883(3)$, $c = 26.232(2)$ Å, as displayed in Fig. 1, similar to the cell constants of $Li_2Sr_{1.5}Nb_3O_{10}$ [21]. This is because the high temperature (1200 °C) led to the departure of Li_2O in the synthesis according to the work of Floros et al. [22], which resulted in the metastable two-layer Ruddlesden–Popper structure collapse to a more stable three-layer Ruddlesden–Popper structure.

Moreover, the reaction was also conducted in different temperatures, such as 1100, 1150, and 1250 °C. When the temperature was below 1200 °C, there are always some impurity in the sample though the $Li_2CaTa_2O_7$ layered structure is very stable in this condition. However, it is hard to obtain pure sample for this two-layered structure, which is very easy to collapse to three-layered structure if the reaction is performed at 1250 °C. In conclusion, 1200 °C is the best temperature for preparing this sample.

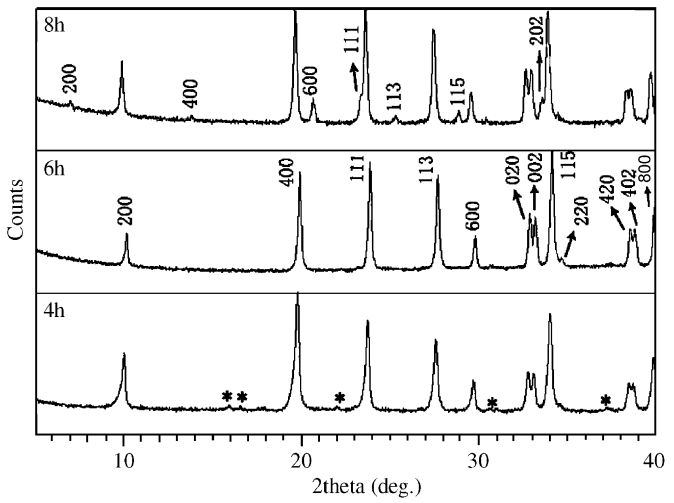

Fig. 1. XRD patterns of $Li_2CaTa_2O_7$ at reaction stages of (a) 4 h, (b) 6 h, and (c) 8 h. The impurity peaks of 4 h were masked by asterisk; the *h k l* of 6 h represent the diffraction peaks of $Li_2CaTa_2O_7$; the *h k l* of 8 h represent the diffraction peaks of $Li_2Ca_{1.5}Ta_3O_{10}$.

3.2. Structure characterization of $Li_2CaTa_2O_7$

For the above synthesis conditions, a pure phase is obtained for the nominal composition $Li_2CaTa_2O_7$. Most of the electron diffraction (ED) investigations performed on more than 10 microcrystals give a similar electron diffraction pattern along the [001] zone axis, which shows that some preference orientations are present in the prepared powder. The HRTEM image (Fig. 2a) indicates that the lattice spacing of 0.552 and 0.546 nm is consistent with that of the (100) and (010) plane in the fast Fourier transformation (FFT) pattern (left inset of Fig. 2a), respectively. The ED pattern of $Li_2CaTa_2O_7$ along the [001] zone axis is shown in Fig. 2b. The ED pattern corresponds to the *ab* plane of the orthorhombic cell, which is consistent with the indexing of the XRD pattern. In the ED pattern (Fig. 2c) of $Li_2CaTa_2O_7$ along the [1$\bar{1}$0] zone axis, diffusing streaks are clearly observed, and are ascribed to the presence of stacking faults. The (002) reflection suggests that the *c*-axis should be doubled, which is consistent with the observed *c* parameter of $Li_2CaTa_2O_7$ [1.82(1) nm] from the XRD pattern. Examination of the ED patterns (Fig. 2) shows a system of intense reflections, characteristic of the orthorhombic cell, with $c\approx18$ Å and $a\approx b\approx a_p\sqrt{2}\approx5.5$ Å, where a_p represents the classic cell parameter of the cubic perovskites subcell. The corresponding reflection conditions, *h k l*, $h+k=2n$, $k+l=2n$ and $h+l=2n$, are compatible with the face-centering structure.

However, there are some complicated phenomena in the ED pattern of Fig. 2b, which should be interpreted carefully: (1) the presence of (210) or (120) extra reflections could be due to the twinning phenomena in the crystallites, which were also observed in the ED patterns of $Li_2SrNb_2O_7$ [22]; (2) the 110 reflections are observed but are always very weak. These extra reflections can be generated by the double-diffraction phenomena as soon as (100) and (010) areas coexist.

All peaks of the XRD pattern (in the angular range $5<2\theta<70°$) could be indexed on an orthorhombic cell [$a\sim5.5153(1)$, $b\sim5.4646(1)$, $c\sim18.2375(3)$ Å] and the systematic absences showing face centering leading to an F-extinction symbol. Thus, we attempted to refine the structure in the space group *Fmmm* with a starting model similar to $Li_2SrNb_2O_7$ [18]. The structure was refined by the Rietveld technique using all data of XRD above 10° (2θ) because of the high asymmetry of background at low angles. For the refinement, with 20 parameters for 259 reflections, we found the conventional reliability factors, R_p, R_{wp}, R_{exp}, R_B, and R_F to be 23.2%, 27.9%, 1.63%, 20.7%, and 9.04%, respectively, which was unsatisfactory. The biggest errors seem to come from the 0 0 1 reflections, always observed to be larger than calculated. Then we applied the March-Dollase option for a correction in the FULLPROF program [19]. The result was greatly improved but still not satisfactory. Finally, we refined 22 parameters including the textured parameter, and we

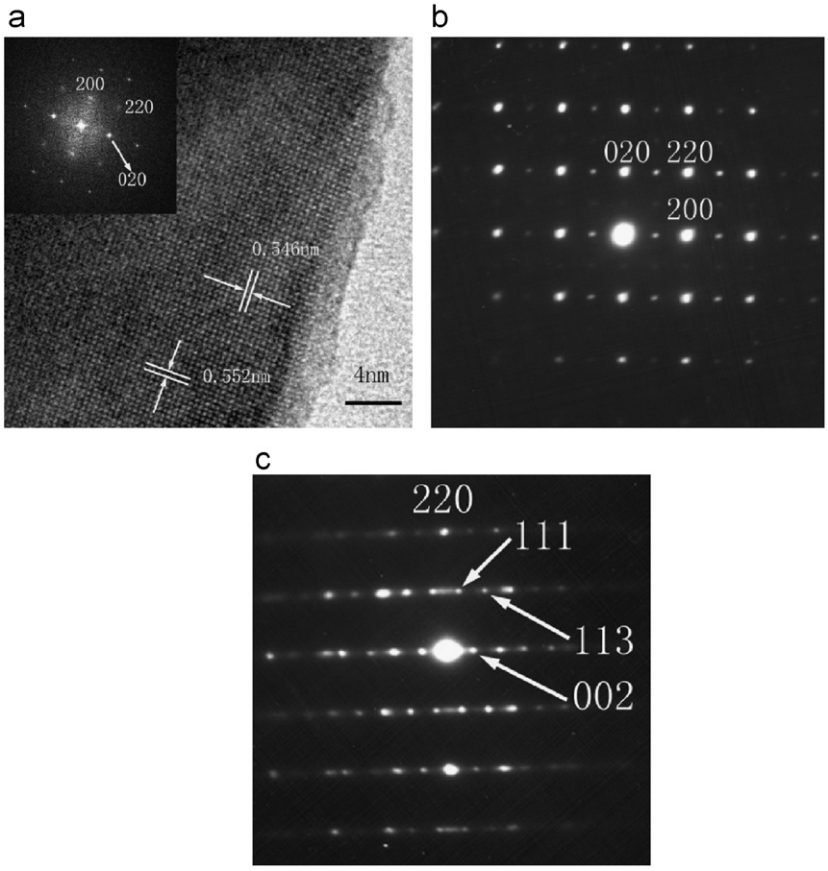

Fig. 2. (a) HRTAM image of $Li_2CaTa_2O_7$ and SAED taken, (b) [001] ED pattern (note that twinning phenomena and double diffraction generate the apparent existence of weak $hk0$ reflection), and (c) [$1\bar{1}0$] ED pattern.

Table 1
The final refined atomic parameters for Rietveld powder X-ray refinement of $Li_2CaTa_2O_7$ in the space group *Fmmm* ($Z = 4$) with $a = 5.5153(1)$, $b = 5.4646(1)$, and $c = 18.2375(3)$ Å

Atom	Site	x	y	z	B/Å^2
Ta	8*i*	0	0	0.38773(3)	0.815(33)
Ca	4*a*	0	0	0	2.157(87)
O(1)	16*j*	$\frac{1}{4}$	$\frac{1}{4}$	0.10036(28)	6.143(123)
O(2)	8*i*	0	0	0.29004(42)	6.143(123)
O(3)	4*b*	0	0	$\frac{1}{2}$	6.143(123)
Li	8*f*	$\frac{1}{4}$	$\frac{1}{4}$	$\frac{1}{4}$	2.838(318)

259 reflections and 22 parameters were used for refinement. $R_p = 9.10\%$, $R_{wp} = 9.22\%$, $R_{exp} = 1.63\%$, $R_B = 4.47\%$, $R_F = 4.06\%$. B values are taken to be the same for all the oxygen atoms. Owing to high asymmetry, the first peak at $2h = 9.714^\circ$ was not taken into consideration in the refinement. The preferential orientation parameter $G_1 = 0.65549(401)$, $G_2 = 0.63421(726)$.

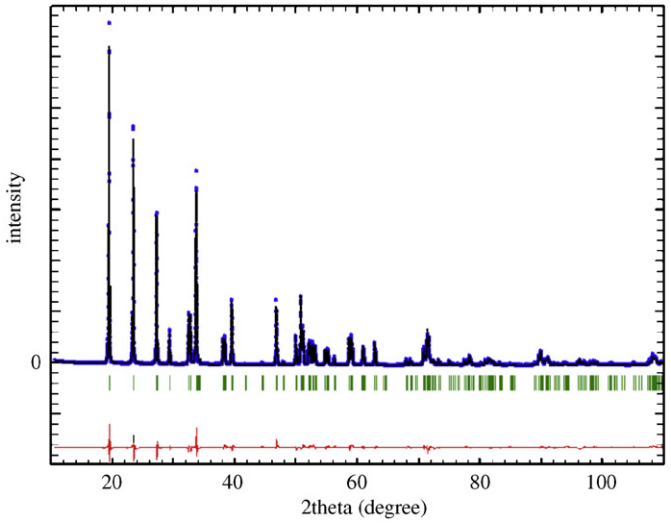

Fig. 3. Experimental (dotted line) calculated and difference (solid lines) powder X-ray diffraction patterns of $Li_2CaTa_2O_7$ after structural refinements in the space group *Fmmm*. The vertical bars are the Bragg positions of the reflections in the space group *Fmmm*.

obtained the best results (Table 1), R_p, R_{wp}, R_{exp}, R_B, and R_F to be 9.10%, 9.22%, 1.63%, 4.47%, and 4.06%, respectively (Fig. 3). While the heavy atoms are probably well located in our model, the X-ray powder data cannot allow a precise determination of the lithium and oxygen atom positions. As already encountered in such compounds, a small displacement of these oxygen atoms leading to a tilting of the octahedral could not be revealed by the powder X-ray diffraction study. Indeed, Floros et al. [22] have carried out structural work on $Li_2SrNb_2O_7$

and $Li_2SrTa_2O_7$, based on powder neutron diffraction experiments. For $Li_2SrNb_2O_7$, their work shows the same super cell and the octahedra tilting in the orthorhombic system (space group *Cmcm*).

A presentation of the $Li_2CaTa_2O_7$ structure is shown in Fig. 4. The structure consists of double layers of corner-sharing TaO_6 octahedra that run perpendicular to the *c*-axis; adjacent sets of layers are staggered as shown in Fig. 4. The TaO_6 octahedra exhibit four very similar equatorial Ta–O bonds (1.9528 Å), whereas along the *c*-axis, a short apical Ta–O distance (1.730 Å) alternates with a longer one (2.0473 Å) corresponding to Ta–O–Li and Ta–O–Ta bonds, respectively. Such a distortion is quite similar to that encountered in homologous niobates and tantalates where the tantalum shows an out-of-plane distortion, moving away from the more positively charged calcium towards the lithium layer. The mean value of the interatomic Ta–O distances, 1.9314 Å, is typical for compounds involving Ta (V). The in-plane and out-of-plane interatomic Ta–Ta distances, 3.882 and 4.095 Å, respectively, show that in the perovskite slabs, the perovskite sub-cell is tetragonally distorted. Similar behavior has been observed in a number of d^0 systems containing niobium, tantalum, and titanium [23,24]. This has been attributed to a second-order Jahn–Teller effect [25]. As a result, the LiO_6 octahedra are strongly distorted with four short and two long Li–O bonds (Table 2), so that the lithium coordination may be described as a regular tetrahedral. The Sr–O distances (Table 2) are close to those commonly observed in perovskites.

Table 2
Selected interatomic distances (Å) for $Li_2CaTa_2O_7$

Li–O(2)	2.093(2)	× 4	Ca–O(1)	2.670(4)	× 8
Li–O(1)	2.726(5)	× 2	Ca–O(3)	2.75760(6)	× 2
Ca–O(3)	2.73225(5)	× 2			
Ta–O(1)	1.9528(6)	× 4			
Ta–O(2)	1.730(5)	× 1			
Ta–O(3)	2.0473(5)	× 1			

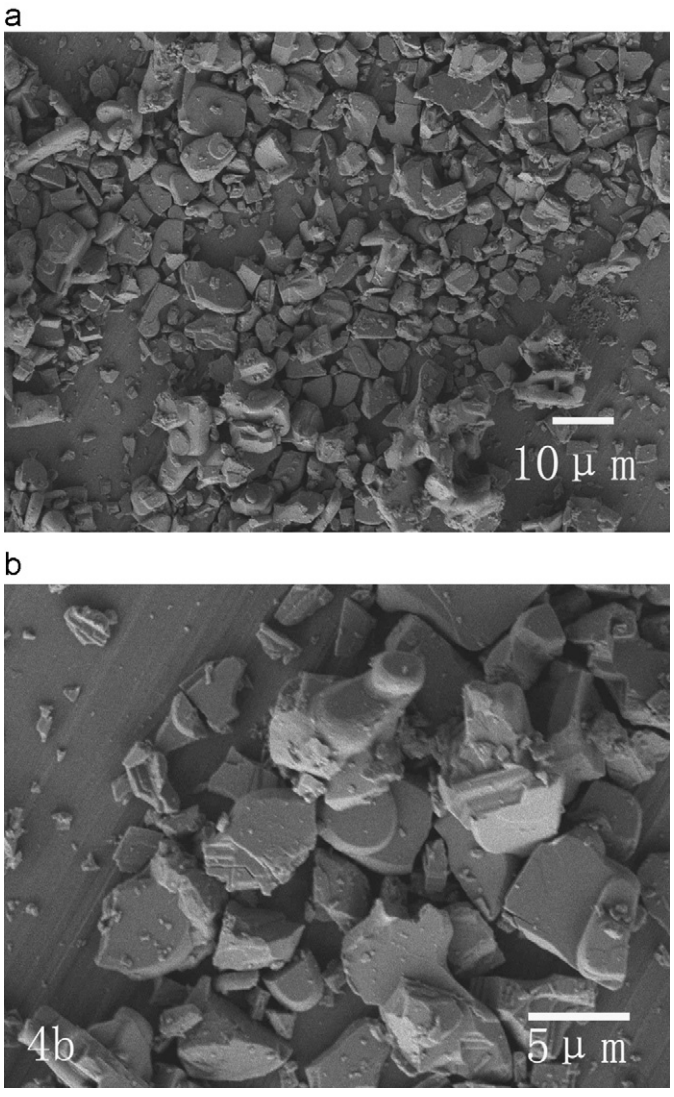

Fig. 4. SEM images of $Li_2CaTa_2O_7$ powders.

Scanning electron micrographs of $Li_2CaTa_2O_7$ powders are shown in Fig. 5. All $Li_2CaTa_2O_7$ powders show an irregular platelike morphology with diameters of 1–10 μm, indicating that there are some platy preference orientation in the XRD pattern.

3.3. Photoabsorption properties and photocatalytic activity of $Li_2CaTa_2O_7$

It is well-known that light absorption by the material and the migration of the light-induced electrons and holes are key factors controlling a photocatalytic reaction, which is relevant to the electronic structure characteristics of the material [26,27]. The photoabsorption ability of the material was detected by UV–vis DRS, as shown in Fig. 6. $Li_2CaTa_2O_7$ presented the photoabsorption properties from the UV-light region to visible light shorter than 450 nm. The steep shape of the spectra indicated that the visible-light absorption was not due to the transition from the impurity level but was due to the band-gap transition. For a crystalline semiconductor, it was shown that the optical absorption near the band edge follows the equation $ahv = A(hv-E_g)^n$, where a, v, E_g, and A are the absorption coefficient, the light frequency, the band gap, and a constant, respectively. Among them, n decides the characteristics of the transition in a semiconductor. According to the equation, the value of n for $Li_2CaTa_2O_7$ was 2 as seen the data in Fig. 5. The band gap of the photocatalyst was estimated to be 4.36 eV from the onset of the absorption edge.

It is known that $Li_2SrTa_2O_7$ has been used as a visible light photocatalyst for photocatalytic water splitting into H_2 and O_2 under UV irradiation [10]. The as-prepared $Li_2CaTa_2O_7$ powders in our approaches have merits such as the two-layer Ruddlesden–Popper structure with interlayer space as reaction sites. Thus, it is reasonable to

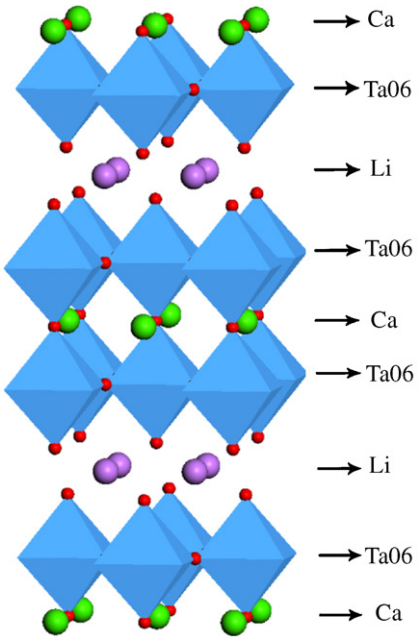

Fig. 5. Crystal structure of a two-layer Ruddlesden–Popper phase $Li_2CaTa_2O_7$.

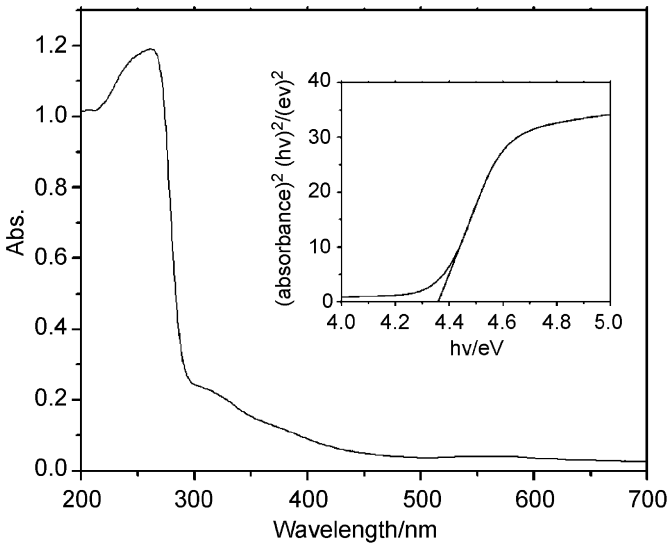

Fig. 6. UV–visible diffuse reflectance spectra of $Li_2CaTa_2O_7$.

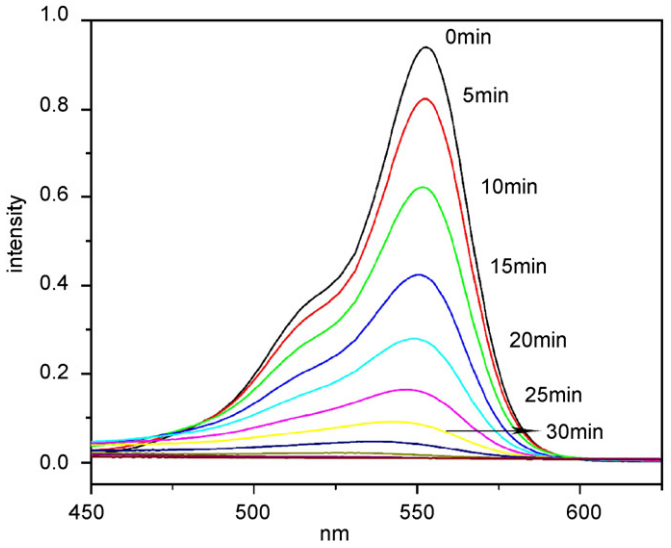

Fig. 7. Absorption changes of RhB solution under photocatalytic process (100 mg $Li_2CaTa_2O_7$ powders added into 200 mL of 2×10^{-5} mol/L RhB solution).

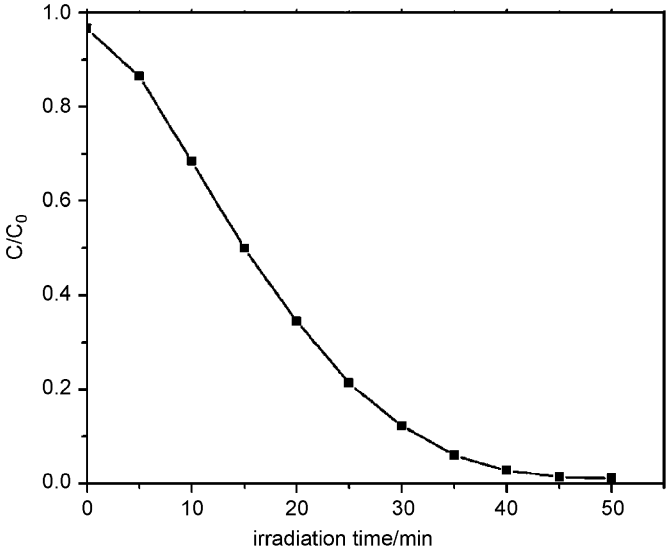

Fig. 8. Photocatalytic degradation of RhB over $Li_2CaTa_2O_7$ particles under UV–vis irradiation lights.

expect that the as-prepared $Li_2CaTa_2O_7$ powders with two two-layer Ruddlesden–Popper structure are ideal photocatalysts. To demonstrate the photocatalytic activity of the $Li_2CaTa_2O_7$ sample for photocatalytic water splitting, we evaluate their photocatalytic activity toward the photodegradation of rhodamine B (RhB) at room temperature as a test reaction. Fig. 6 displays the temporal evolution of the spectra during the photodegradation of RhB (initial concentration: 2×10^{-5} M, 200 mL) in the presence of the $Li_2CaTa_2O_7$ sample under UV–vis light illumination. The absorption peaks at 553 nm corresponding to RhB diminished gradually with an absorption band shift to shorter wavelengths as the exposure time was extended. In the process of photodegradation of RhB by $Li_2CaTa_2O_7$, the intense pink color of the starting RhB solution gradually faded. Fig. 7 displays the temporal evolution of the spectra during the photodegradation of RhB mediated by the $Li_2CaTa_2O_7$ sample under UV–vis light illumination. The photodegradation efficiency of RhB as a function of irradiation time is shown in Fig. 8 which indicates that the absorption peaks corresponding to RhB completely disappeared after about 50 min. Thus, such materials with interesting properties represent good candidates for further applications in the fields of photocatalytic science and technology.

4. Conclusion

In summary, a new two-layer Ruddlesden–Popper phase $Li_2CaTa_2O_7$ has been synthesized for the first time using solid-state reactions. The $Li_2CaTa_2O_7$ powders crystallize in the space group *Fmmm* [$a\sim5.5157(3)$, $b\sim5.4652(3)$, $c\sim18.2338(9)$ Å]. The fabricated functional semiconductor exhibits photocatalytic activity in the degradation of RhB. It is expected that this kind of two-layer Ruddlesden–Popper structure $Li_2CaTa_2O_7$ could be used for applications in photocatalytic cleaners, optoelectronic devices, water purification, environmental cleaning, and solar energy conversion. This work could be of great importance in extending the potential applications of $Li_2CaTa_2O_7$, a potential advanced functional material.

Acknowledgments

Financial support by the National Natural Science Foundation of China (No. 20621061), the 973 Projects of China and the Program for New Century Excellent Talents in university (NCET) are gratefully acknowledged.

References

[1] P.A. Salvador, K.B. Greenwod, J.R. Mawdsley, K.R. Poeppelmeier, T.O. Mason, Chem. Mater. 11 (1999) 1760–1770.
[2] K.L. Kobayashi, T. Kimura, H. Sawada, K. Terakura, Y. Tokura, Nature 395 (1998) 677–680.
[3] P.W. Rehrig, S.E. Park, S. Trolier-McKinstry, G.L. Messing, B. Jones, T.R. Shrout, J. Appl. Phys. 86 (1999) 1657–1661.
[4] M.A. Pena, J.L.G. Fierro, Chem. Rev. 101 (2001) 1981–2017;
M. Machida, J. Yabunaka, T. Kijima, Chem. Mater. 12 (2000) 812–817.
[5] M. Dion, M. Ganne, M. Tournoux, Mater. Res. Bull. 16 (1981) 1429–1435;
A.J. Jacobson, J.W. Johnson, J.T. Lewandowski, Inorg. Chem. 24 (1985) 3727–3729.
[6] S.N. Ruddlesden, P. Popper, Acta Crystallogr. 10 (1957) 538–539;
S.N. Ruddlesden, P. Popper, Acta Crystallogr. 11 (1958) 54–55.
[7] B. Aurivillius, Ark. Kemi 1 (1949) 463–480;
B. Aurivillius, Ark. Kemi 1 (1949) 499–512;
B. Aurivillius, Ark. Kemi 2 (1950) 519–527.
[8] P.J. Olliver, T.E. Mallouk, Chem. Mater. 10 (1998) 2585–2587.
[9] R.E. Schaak, T.E. Mallouk, Chem. Mater. 12 (2000) 3427–3434.
[10] K. Shimizu, Y. Tsuji, T. Hatamachi, K. Toda, T. Kodama, M. Sato, Y. Kitayama, Phys. Chem. Chem. Phys. 6 (2004) 1064–1069;
K. Shimizu, S. Itoh, T. Hatamachi, T. Kodama, M. Sato, K. Toda, Chem. Mater. 17 (2005) 5161–5166.
[11] T. Tanaka, Y. Furumi, K. Shinohara, A. Tanaka, M. Hara, J.N. Kondo, K. Domen, Chem. Mater. 9 (1997) 1063–1064.
[12] K. Sayama, A. Tanaka, K. Domen, K. Maruya, T. Onishi, J. Phys. Chem. 95 (1991) 1345–1348.
[13] A. Kudo, H. Kato, Chem. Lett. 26 (1997) 867–868;
T. Ishihara, H. Nishiguchi, K. Fukamachi, Y. Takita, J. Phys. Chem. B 103 (1999) 1–3.
[14] A. Kudo, H. Kato, S. Nakagawa, J. Phys. Chem. B 104 (2000) 571–575.
[15] H. Kato, A. Kudo, J. Phys. Chem. B 105 (2001) 4285–4292.
[16] A. Kudo, H. Kato, J. Am. Chem. Soc. 125 (2003) 3082–3089;
Z. Zou, J. Ye, K. Sayama, H. Arakawa, Nature 414 (2001) 625–627.
[17] T.A. Kodenkandath, J.B. Wiley, Mater. Res. Bull. 35 (2000) 1737–1742;
M.P. Crosnier-Lopez, F. Le Berr, J.L. Fourquet, J. Mater. Chem. 11 (2001) 1146–1151.
[18] N.S.P. Bhuvanesh, M.P. Crosnier-Lopez, H. Duroy, J.L. Fourquet, J. Mater. Chem. 9 (1999) 3093–3100.
[19] J. Rodriguez-Carvajal, FULLPROF Program: Rietveld Pattern Matching Analysis of Powder Patterns, ILL Grenoble, 1990.
[20] R.D. Shannon, Acta Crystallogr. A 32 (1976) 751–767.
[21] N.S.P. Bhuvanesh, M.P. Crosnier-Lopez, O. Bohnke, J. Emery, J.L. Fourquet, Chem. Mater. 11 (1999) 634–641.
[22] N. Floros, C. Michel, M. Hervieu, B. Raveau, J. Mater. Chem. 9 (1999) 3101–3106.
[23] K. Toda, T. Teranishi, M. Takahashi, Z.G. Ye, M. Sato, Solid State Ionics 113 (1998) 501–508.
[24] S.H. Byeon, S.O. Lee, H. Kim, J. Solid State Chem. 130 (1997) 110–116.
[25] N.S.P. Bhuvanesh, J. Gopalakrishnan, J. Mater Chem. 7 (1997) 2297–2306.
[26] J.W. Tang, Z.G. Zou, J.H. Ye, Angew. Chem. Int. Ed. 43 (2004) 4463–4466.
[27] J.W. Tang, Z.G. Zou, J.H. Ye, Chem. Mater. 16 (2004) 1644–1649.